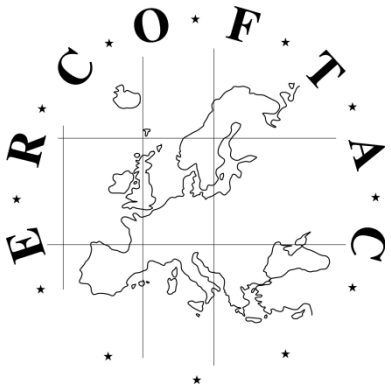


ERCOFTAC
Classic Collection Database

# COMBINED FLOW AND DEFLECTION MEASUREMENTS OF FSI-INDUCED OSCILLATION OF TWO RIGID STRUCTURES IN TURBULENT FLOWS

*in section* Flows Around Bodies / Two-dimensional flows / 7. Around oscillating bodies or with unsteady approach flow

Author(s):
**JORGE PEREIRA GOMES and HERMANN LIENHART**
2011 • EXPERIMENTAL

Institute of Fluid Mechanics and
Erlangen Graduate School in Advanced Optical Technologies,
University of Erlangen-Nuremberg,
Cauerstrasse 4, D-91058 Germany
jgomes@lstm.uni-erlangen.de / lienhart@lstm.uni-erlangen.de

# 1. Description

Characterisation of the FSI-induced two-dimensional limit-cycle oscillation (LCO) of two rigid structures in pure rotation in uniform flows. The measurements were performed in water at a constant flow velocity of *1,07* m/s.

# 2. Geometrical parameters

## *2.1 Models definition*

The structure models are presented in figure 2.1. The first model consisted of a simple *2* mm thick carbon-reinforced fiber flat plate. The second model consisted of a front *22* mm diameter aluminium circular cylinder with an attached flat plate. For simplicity, the same kind of plate was used for this model, i.e., a *2* mm carbon-reinforced fiber plate. The overall length of the models was defined as *64* mm and the spanwise dimension was chosen to be equal to the spanwise dimension of the test section and to guarantee the two-dimensionality of the experiments. Just a small gap of *1,5* mm between the models and the walls of the test section was set in order to avoid any possible friction between the moving models and the walls.

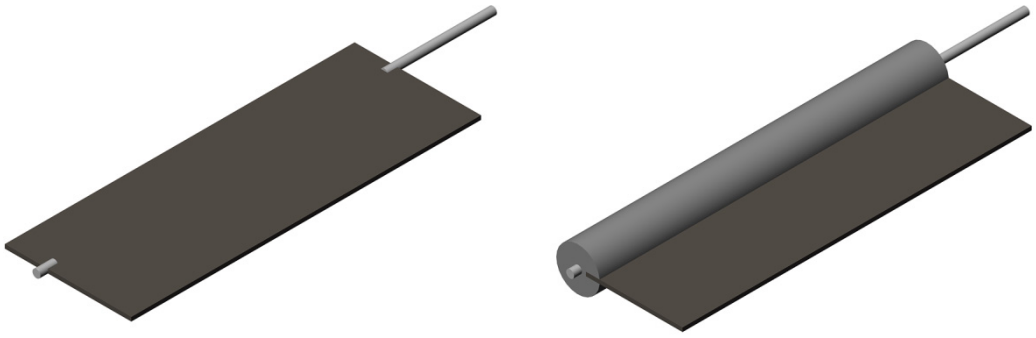

*Figure 2.1 – Rigid structure models.*

The geometric definition of the models is presented in figure 2.2. Table 2.1 summarizes the mechanical and dynamic properties of these models.

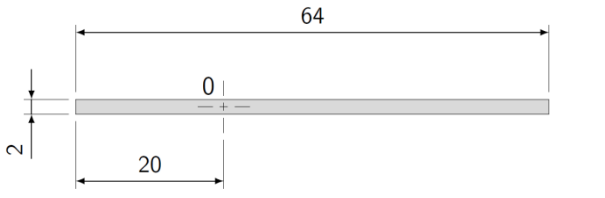


(a) PC1 model

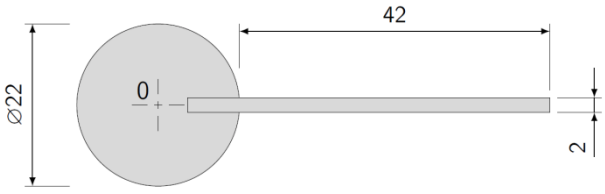


(b) CC1 model

*Figure 2.2 – Geometry of the models (dimensions in mm).*

| | PC1 model | CC1 model |
|---|---|---|
| $\rho_{front\ body}$ [kg/m$^3$] | - | *2828* |
| $\rho_{flat\ plate}$ [kg/m$^3$] | *1475* | *1475* |
| | | |
| $m$ [g] | *33,4* | *208,9* |
| $I_0$ [kg m$^2$] | *1,62E-5* | *3,70E-5* |
| $x_{CM}$ [mm] | *12,00* | *3,49* |
| $f_0$ [Hz] | *2,48* | *2,21* |

*Table 2.1 – Property values of the structure model.*

### *2.2 Flow domain definition*

The measurements were conducted in a vertical, closed-loop water tunnel. The spatial dimensions of the tunnel test section are presented in figure 2.3. It had a *180* mm × *240* mm cross-sectional area and a total length of *380* mm. As a direct consequence of the vertical orientation of the tunnel, the gravity force was aligned with the flow ($x$-axis, see figure 2.3). In this way, the gravity force did not introduce any asymmetry in the experiments. All test models were mounted *55* mm downstream of the inlet plane of the test section with a free rotational degree-of-freedom. The supporting system used two low friction bearings and was designed to guarantee frictionless rotation of the model around the $z$-axis (see figure 2.3).

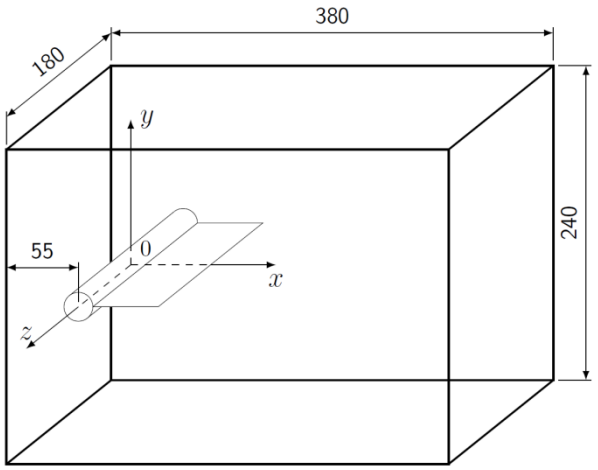


*Figure 2.3 – Test section geometry (dimensions in mm).*

## 3. Flow parameters

The fluid properties for the two test cases were identical and are summarized in table 3.1. Within the temperature range of the tests, the kinematic viscosity and density of the fluid were measured to be constant.

| Test case | $U_\infty$ [m/s] | Re [-] | $\nu$ [m$^2$/s] | $\rho$ [kg/m$^3$] |
|---|---|---|---|---|
| PC1 | *1,07* | *70600*[(a)] | *0,97E-6* | *998* |
| CC1 | *1,07* | *24300*[(b)] | *0,97E-6* | *998* |

[(a)] based on the overall length of the model.
[(b)] based on the diameter of the front body of the model.

*Table 3.1 – Flow parameters.*

The inlet velocity condition was characterized in the absence of any model at the location $x$ = *-55* mm in the centre plane of the test section ($z$=*0* mm, see figure 2.3). The flow angularity was measured to be less than *0,5°* and the RMS value associated with the fluctuation of the magnitude of the velocity less that *1%*. These values, and also the mean flow velocity, corresponded to the interval *-85* mm $\leq y \leq$ *85* mm.

The inlet velocity profile for the test cases is available in the following file:

| test case | file name | quantities |
|---|---|---|
| PC1 and CC1 ($U_\infty = 1{,}07$ m/s) | C1_Inlet_Velocity_Profile.txt | $U_\infty(y)$ |

Example:

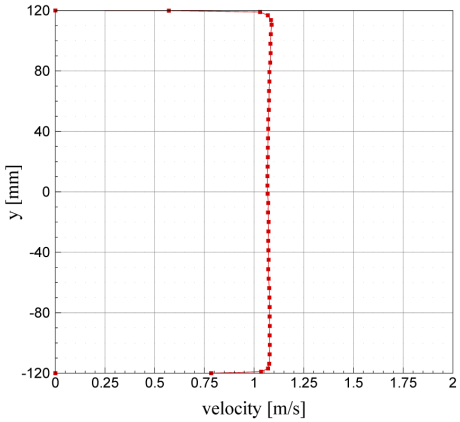


*Figure 3.1 – File C1_Inlet_Velocity_Profile.txt.*

## 4. Experimental details

### *4.1 Flow field measurements*

The flow velocity field was measured using a DANTEC two-dimensional, two-component particle image velocimetry (PIV) system. For the acquisition of the images, two synchronized *1280* pixel × *1024* pixel CCD cameras equipped with *60* mm focal length macro lenses were adopted to acquire two simultaneous and adjacent time-dependent pairs of images from the centre plane of the test section (*xy*-plane, see figure 2.3). The PIV images acquired by the two cameras were then imported into a MatLab-based post-processing script to stitch the corresponding pairs of images before being correlated. Opting for this solution, it was possible to achieve an extended *270* mm × *170* mm flow field measuring area while keeping the spatial resolution of the measurements as high as *7,53* CCD pixel/mm.

For the ilumination of the flow, two laser light sources were used from both sides of the test section, each to illuminate the flow at each side of the model, and, therefore, to avoid any shadow region in the flow. The lasers were of the double-head pulsed Nd:YAG type and delivered light pulses of a wavelength of *532* nm with a maximum energy of *120* mJ.

As seeding particles, *10* μm mean diameter hollow glass spheres were chosen.

### *4.2 Reconstruction of the measurements in the time-phase space*

The measuring system was operated at constant acquisition rate and the reconstruction of the measurements in the time-phase space was performed during the post-processing period. This approach was chosen instead of triggering the data acquisition by the experiment in order to coupe with the usual cycle-to-cycle fluctuation of the structure oscillation period found in free oscillation tests. Figure 4.1 shows a typical data reconstruction using this method. Simultaneously with the acquisition of the measurements, two kind of events, the acquisition of the measurements $tm_i$ [figure 4.1(B)] and the beginning of the movement cycles $tc_j$ [figure 4.1(A)], were recorded. These time events were detected using the camera trigger signal and the signal of an angular position sensor located in the rotating axle of the structure, respectively. The event monitoring was performed by an hardware module designed based on a field programmable gate array (FPGA) and a *1* MHz internal clock. It was capable to record up to *250* events per second with an accuracy of *2* μs.

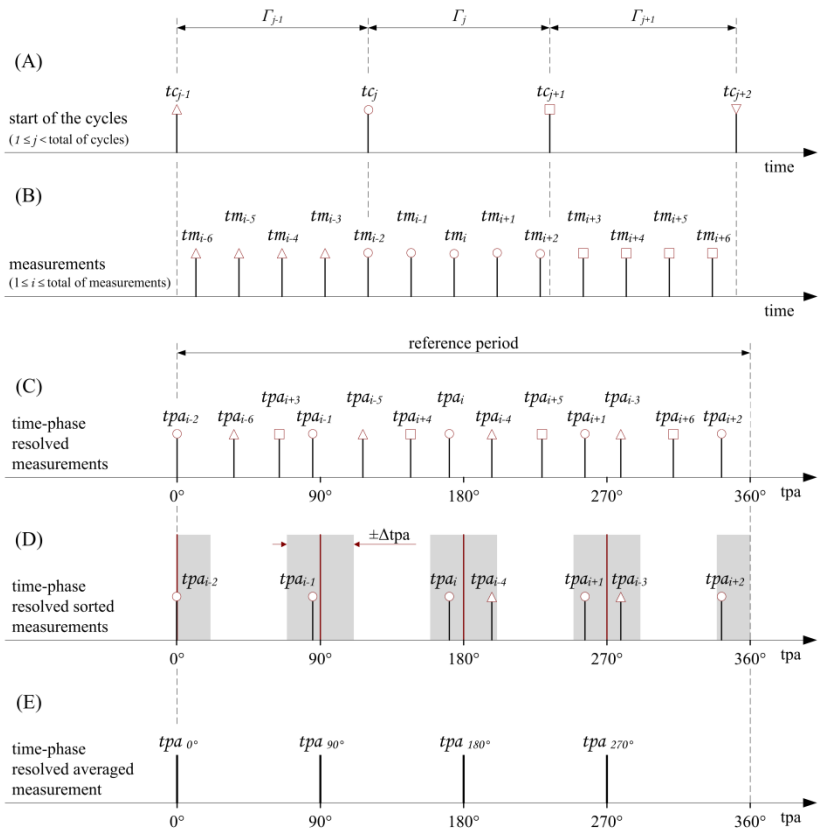


*Figure 4.1 – Time-phase resolved measurements reconstruction scheme.*

From the recorded events time information, a post-processing software computed the time-phase angle $\varphi$ for each acquired measurement. At this point, the resolved measured data could be reorganized in a reference period $\bar{\Gamma}_j$ equal to the mean period of all acquired cycles [figure 4.1(C)] to be sorted out according to a predefined time-phase angle resolution and uncertainty [figure 4.1(D)]. Finally, the data falling within one time-phase angle slot were averaged to obtain the final result [figure 4.1(E)]. In the present test cases, the reconstruction of the experimental results was performed with a time-phase resolution and uncertainty of *5°* and *0,5°*, respectivelly, and the final result corresponded to the mean value of *100* realizations.

## 5. Experimental data

All data corresponding to the present test cases can be downloaded as a single file as follows:

| |
|---|
| C_Data_All_Files.rar |
| C_Data_All_Files.gz |
| C_Data_All_Files.7z |

All experimental results are organized in the test cases. Table 5.1 shows the frequency of the limit cycle oscillation of the model together with the RMS value associated with the cycle-to-cycle fluctuation registered during the data acquisition.

| | |
|---|---|
| PC1 | *2,49* Hz *±1,8* % |
| CC1 | *5,08* Hz *±1,3* % |

*Table 5.1 – Oscillation frequency of the model.*

The time-phase trace of the angle of the model ($\theta$) within an oscillation period is available in the following files:

| test case | file name | quantities |
|---|---|---|
| PC1 | PC1_Structure_Angle.txt | $\theta(\varphi)$ |
| CC1 | CC1_Structure_Angle.txt | $\theta(\varphi)$ |

Example:

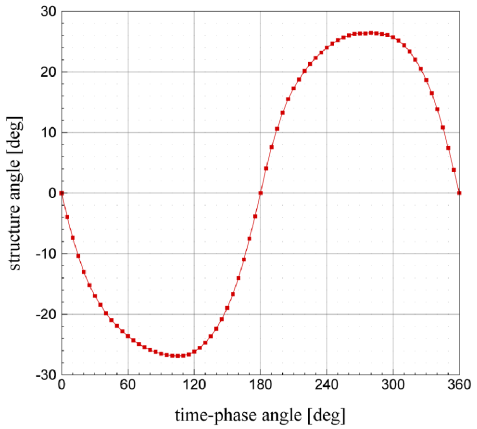


*Figure 5.1 – File PC1_Structure_Angle.txt.*

The time-phase resolved data on the flow velocity field is available in the following packages:

| test case | file name | quantities |
|---|---|---|
| PC1 | PC1_tpa_Files.rar | $u(\varphi;x;y)$ ; $v(\varphi;x;y)$ ; $(u^2+v^2)^{1/2}(\varphi;x;y)$ |
| CC1 | CC1_tpa_Files.rar | $u(\varphi;x;y)$ ; $v(\varphi;x;y)$ ; $(u^2+v^2)^{1/2}(\varphi;x;y)$ |

Each package contains *72* files correspondent to different time-phase angles within an oscillation period. The experimental results obtained at the beginning of the oscillation period ($\varphi=0°$) are stored in the file *_0000.txt*, and the final measuring point corresponded to $\varphi=355°$ and the results are stored in the file named *_3550.txt*. The intermediate measuring points were defined with a time-phase resolution of *5°* and the results for $\varphi=360°$ are identical to those for $\varphi=0°$. The files also considered a prefix which identifies the test case the files belong. For example, file *PC1_0450.txt* corresponds to the test case PC1 and contains the results obtained for the time-phase angle $\varphi=45°$.

About the flow velocity field results, the measuring location was set to the middle plane of the experimental domain ($z=0$, see figure 2.3) and considered a *270* mm × *170* mm rectangular measuring area. The area, which extended from $-35$ mm up to *235* mm in the $x$-direction and from $-85$ mm up to *85* mm in the $y$-direction, is represented in figure 5.3. The spatial resolution of the velocity field measurements was defined as *2,1* mm and the accuracy associated with them was measured better than *1,5%* for the undisturbed flow. Both the $u$- and $v$-components and also the magnitude of the velocity were normalized by the free stream flow velocity, $U_\infty$.

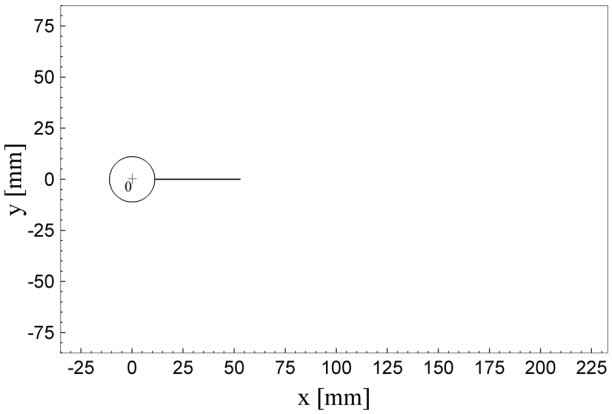


*Figure 5.3 –Measuring area.*

Finally, one should take into account that the results obtained with the PC model were affected by the supporting system of the structure. In this case, the structure was not large enough to overlap the image of the bearing holder and therefore the part of the flow field correspondent to the *13* mm diameter circle arround the origin was not accessible by optical means. In figure 5.4, the area corresponding to the bearing holder where no measurements could be performed is represented by a black circle.

Example:

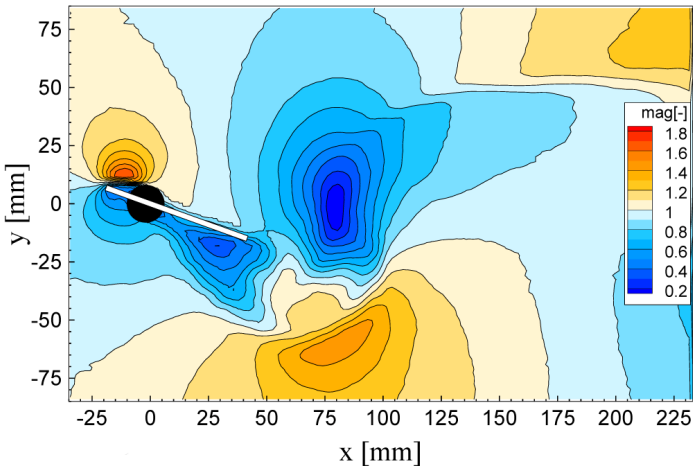


*Figure 5.4 – File PC1_0450.txt.*

## Acknowledgements

The authors gratefully acknowledge the financial support for their research work through the German Science Foundation (DFG), Germany, and Fundação para a Ciência e a Tecnologia (FCT), Portugal. In addition, the authors acknowledge the funding of the Erlangen Graduate School in Advanced Optical Technologies (SAOT) by DFG in the framework of the German excellence initiative.

## References

[1] Gomes, J. P. (2011) *Fluid-structure interaction-induced oscillation of flexible structures in uniform flows*, Ph.D. Thesis.

[2] Gomes, J. P. and Lienhart, H. (2009) Experimental Benchmark: Self-excited Fluid-structure Interaction Test Cases, in *Fluid-Structure Interaction II: Modelling, Simulation, Optimisation*, Bungartz, H. J., Mehl, M., Schäfer, M. (eds.), **383-412**, Springer-Verlag.